Water Vapor Correction Method for Advanced Very High Resolution Radiometer Data

MOIRA L. STEYN-ROSS, D. A. STEYN-ROSS, P. J. SMITH AND J. D. SHEPHERD

Physics Department, University of Waikato, Hamilton, New Zealand

J. REID AND P. TILDESLEY

Commonwealth Scientific and Industrial Research Organisation Marine Laboratories, Hobart, Tasmania, Australia

Current sea surface temperature (SST) retrieval algorithms consist of linear equations involving brightness temperatures (of the infrared advanced very high resolution radiometer (AVHRR) channels) multiplied by fixed coefficients a_i. These coefficients are derived from atmospheric transmission models and radiosonde profiles or from regression against ocean buoy measurements. Errors in SST retrieval occur when the actual atmospheric conditions differ from those assumed when the a_i were originally computed; it is generally agreed that water vapor variations are the primary source of this error. We propose a novel radiance-based SST algorithm which compensates for temporal fluctuations in the water vapor profile. The method does not use any form of regression; rather, we utilize a single radiosonde seed combined with full radiative transfer theory applied to an atmospheric model. As well as improving the accuracy of the remotely sensed SST, this approach allows us to estimate the total water vapor content for a given AVHRR pixel. We compare the performance of this technique with two standard SST models, using buoy data from the west coast of Tasmania as surface truth. Preliminary results from a sample of 33 NOAA 9 overpasses gathered over a 10-month period in 1987 are most encouraging: the dynamic water vapor (DWV) algorithm outperforms the standard SST methods in terms of retrieval accuracy, underestimating the buoy temperature by an average of 0.22 K. This result demonstrates that the method has merit and suggests that the total water vapor content returned by the DWV algorithm is probably a reasonable first estimate.

1. INTRODUCTION

There are several methods for estimating sea surface temperatures (SSTs) from advanced very high resolution radiometer (AVHRR) data. *McClain et al.* [1985] provide a review of recent techniques; typically, SST is computed from a linear combination of brightness temperatures measured by AVHRR channels 3, 4, and 5 (centered at 3.7, 11, and 12 μm, respectively) of the National Oceanic and Atmospheric Administration (NOAA) series of meteorological satellites.

A detailed discussion of the theoretical basis of multiple-window SST retrievals is given by *McMillin and Crosby* [1984]. In essence, all retrieval methods are based on the equation of radiative transfer for a clear atmosphere, which, using the mean-value approximation, states

$$I_v = B_v(T_s)\,\tau_{v,\infty} + B_v(\overline{T}_a)(1-\tau_{v,\infty}) \tag{1}$$

where I_v is the upwelling radiance sensed by the satellite at a wavenumber v, $B_v(T_s)$ is the Planck function at the surface temperature, $\tau_{v,\infty}$ is the transmittance of the entire atmosphere, $\overline{T}_a$ is the average atmospheric temperature, and

$$B_v(\overline{T}_a) = \frac{\int_{\tau_s}^{1} B_v(T(p))\,d\tau_v(p)}{\int_{\tau_s}^{1} d\tau_v(p)} \tag{2}$$

describes the average atmospheric radiance, with $\tau_v(p)$ as the transmittance at pressure level p.

If we make the assumption that the mean atmospheric temperature $\overline{T}_a$ for AVHRR channel 4 is the same as that for channel 5, we can expand the Planck function for channel 4 as a function of the Planck function for channel 5 to obtain an expression for the blackbody radiance of the surface I_s as

$$I_s = I_4 + \gamma(I_4 - I_{4,5}) \tag{3}$$

where I_4 is the measured radiance in channel 4, $I_{4,5}$ is the radiance at the wavelength of channel 4 that has the same brightness temperature as the radiance measured in channel 5, and γ is the transmissivity ratio

$$\gamma = (1 - \tau_{4,\infty})/(\tau_{4,\infty} - \tau_{5,\infty}) \tag{4}$$

Because of its apparently complicated form, (3) has only rarely been used as an SST retrieval algorithm. To produce a simpler algorithm, it is usual to make a further approximation, namely, that the surface and atmospheric temperatures are approximately equal: $\overline{T}_a \approx T_s$ = SST. One may then perform a Taylor expansion on equation (1) in temperature space to obtain

$$T_s = T_{b,4} + \gamma(T_{b,4} - T_{b,5}) \tag{5}$$

where $T_{b,4}$ and $T_{b,5}$ are the brightness temperatures in channel 4 and 5, respectively.

From inspection of either (3) or (5) it is clear that the accuracy (or otherwise) of the assumed value for the γ transmissivity ratio is the major factor limiting an accurate SST retrieval. As shown by *McClain et al.* [1985], if the transmittance is approximated by an exponential in water vapor amount, then γ becomes, to first order, a constant, and to second order, a linear function of water vapor amount.

In practice, one often uses a climatological average generated by applying a suitable transmission model to a set of atmospheric profiles appropriate to the time and location of interest. One then forms a regression fit of $(T_s - T_{b,4})$ against $(T_{b,4} - T_{b,5})$ to produce an SST algorithm of the form

$$\text{SST} = T_s = T_{b,4} + a_1(T_{b,4} - T_{b,5}) + a_2 \qquad (6)$$

where a_1 and a_2 are fitted constants. Alternatively, these coefficients can be generated empirically by performing a regression fit of AVHRR data with matched buoy measurements.

None of these theoretical or empirical regression models can produce accurate SST retrievals if the prevailing atmospheric conditions (hereafter referred to as the actual atmosphere) are substantially different from the atmospheric conditions used to obtain a_1 and a_2 (hereafter referred to as the assumed atmosphere). Errors resulting from mismatches between the actual and the assumed atmospheres will be reduced if the coefficients a_i are periodically updated using atmospheric data as they become available. This updating should compensate for variations in the atmospheric temperature profiles, since the profiles stay relatively constant over time periods of the order of a month. However, the water vapor content of the atmosphere is a highly variable quantity, especially over the sea, and exhibits large day-to-day fluctuations. These fluctuations produce equivalent fluctuations in the γ parameter appearing in (5), causing fixed-coefficient algorithms to yield inaccurate SST estimates. Thus a more systematic way of dealing with water vapor variability is required. Several approaches have been suggested.

Barton et al. [1989] formulate a regression-fitted algorithm which corrects for both water vapor absorption and zenith angle dependence. *McClain et al.* [1985] describe how the coefficients can be fine-tuned using floating buoy measurements, thus permitting the SST algorithms to be continually recalibrated for those regions containing buoys within the AVHRR coverage zone. The intrinsic limitation of this method is that it cannot readily be generalized to the global scale, since vast expanses of the world's oceans contain no buoys, and unfortunately, these fine-tuned algorithms are likely to be valid only in the region local to the buoy. There is also the secondary problem that while the buoy monitors bulk sea temperature, the satellite radiometer senses the skin temperature of the top few microns of the water surface; at present, the relationship between the bulk and skin temperatures is not well understood.

Another approach that addresses the problem of atmospheric water vapor is the cross-product method of *Walton* [1988], which uses a pair of single-channel equations of the form $T_{s,i} = a_i T_{b,i} + b_i$ ($i = 4, 5$ is the channel number; the coefficients a_i and b_i have been obtained by some form of regression) to derive a pair of SST estimates, $T_{s,4}$ and $T_{s,5}$, from the corresponding brightness temperature pair $T_{b,4}$ and $T_{b,5}$. Plot the points $(T_{s,4}, T_{b,4})$ and $(T_{s,5}, T_{b,5})$ on a graph of $T_{s,i}$ versus $T_{b,i}$; join these points with a line, and extrapolate to the line $T_{s,i} = T_{b,i}$ (representing a channel with no atmospheric absorption). The intersection point represents the final estimate for the SST. The underlying assumption is that there is a linear relationship between the predictions of the two real channels and that of an imaginary, ideal channel which is unaffected by atmosphere. This technique has

met with considerable success, producing more accurate SSTs than other multichannel methods [*Walton et al.*, 1990].

As noted by *Walton* [1988] in his description of the cross-product method, the pair of surface temperature estimates $T_{s,4}$ and $T_{s,5}$, as obtained from the pair of single-channel regression equations, can be equal only if the assumed and actual atmospheric profiles are identical. We build on this fundamental observation to construct a more general, physics-based SST retrieval technique which corrects for temporal atmospheric water vapor fluctuations. We assume that any deviation between our assumed and the actual atmosphere, as detected by a nonzero $(T_{s,4} - T_{s,5})$ difference, primarily arises from variations in water vapor content, so we adjust the assumed water vapor profile iteratively until the pair of SST estimates $T_{s,4}$ and $T_{s,5}$ agree. This dynamic tuning of the atmosphere not only produces a more accurate final SST estimate, but also allows us to estimate the atmospheric water vapor content.

We use the LOWTRAN 7 atmosphere-modeling software [*Kneizys et al.*, 1988] to compute the predicted $(T_{s,4} - T_{s,5})$ mismatch as a function of the difference between the assumed and actual water vapor profiles. We find that the greater the water profile difference, the greater the resulting mismatch between the channel 4 and 5 SST predictions. The fact that this temperature mismatch turns out to be an approximately linear function of total water vapor content discrepancy confirms the validity of our method.

In the following sections we describe our dynamic water vapor (DWV) method in some detail and then compare its performance with two standard retrieval methods: the M4 [*McMillin and Crosby*, 1984] multichannel algorithm (MCSST) and the National Environmental Satellite and Data Information Service (NESDIS) cross-product (CPSST) method [*Walton et al.*, 1990]. We use buoy measurements as "surface" truth.

2. DYNAMIC WATER VAPOR CORRECTION ALGORITHM

We observe that for infrared remote-sensing purposes, the water vapor content is the most significant and most rapidly varying component of the atmosphere. We therefore conjecture that any mismatch between our model atmosphere and the actual atmospheric condition is primarily due to errors in the assumed water vapor profile. We assume that the difference $\Delta\text{SST} = (T_{s,4} - T_{s,5})$, where $T_{s,4}$ and $T_{s,5}$ are the pair of SST estimates obtained from (1) using the radiances in channels 4 and 5, respectively, provides a measure of how much the assumed and actual water vapor profiles differ. If there is no error in the assumed water profile, we would expect $(T_{s,4} - T_{s,5}) = 0$, in which case the actual SST $= T_{s,4} = T_{s,5}$. We use this idea to generate an "algorithm correction" look-up table, as described below.

Rather than using the standard temperature approximation of (5), we compute brightness temperatures directly from the radiance equation (1), and therefore do not require either of the simplifying assumptions implicit in (5); thus the channel 4 and 5 average atmospheric temperatures need not be equal, and more significantly, the sea surface temperature need not be set equal to the average atmospheric temperature. This latter relaxation allows our model to compute distinct values for the average atmospheric temperatures in channels 4 and 5 as well as the sea surface temperature.

In the unlikely event that the transmittance $\tau_{v,\infty}$ and atmospheric radiance $B_v(\bar{T}_a)$ for both channels ($v = 4, 5$) are

known exactly, (1) will yield a single unambiguous value for the SST. In the more usual case, reasonable first guesses for $\tau_{v,\infty}$ and $B_v(\overline{T}_a)$ are the best we can hope for, leading to a pair of SST estimates, $T_{s,4}$ and $T_{s,5}$, whose closeness (or otherwise) indicates the quality of the guessed transmittance and atmospheric radiance. In our case, we compute first-guess values for $\tau_{v,\infty}$ and $B_v(\overline{T}_a)$ for our region of interest (over an ocean buoy off the west coast of Tasmania) by running the LOWTRAN 7 atmospheric transmission model initialized with radiosonde profiles recorded at Hobart (southeastern Tasmania). Since the surface temperature at Hobart is unlikely to match the ocean surface temperature, we set our first guess for the ocean temperature to be equal to the monthly average SST obtained from climatological archives.

Creating the DWV Correction Table

We first create a look-up table of water vapor adjustments by systematically perturbing the original radiosonde profile with the addition of successively larger and larger amounts of water vapor, computing the resulting mismatch between channel 4 and 5 SST estimates. In actual application, the completed table is used in reverse: Given that there is a mismatch between the SST retrievals in the two infrared channels, by how much must the water vapor profile be adjusted in order to cancel this apparent $(T_{s,4} - T_{s,5})$ temperature difference?

Follow steps 1 to 4 create the look-up table.

1. Calculate the initial values for the transmissivity $\tau_{v,\infty}^\circ$ and atmospheric radiance $B_v^\circ(\overline{T}_a)$ for channels 4 and 5 using LOWTRAN 7 initialized with the radiosonde profiles. Call ($\tau_{4,\infty}^\circ$, $\tau_{5,\infty}^\circ$) and ($B_4^\circ(\overline{T}_a)$, $B_5^\circ(\overline{T}_a)$) the prescribed algorithm coefficients.

2. Maintain the same temperature profile as used in step 1, but adjust the water vapor profile by assuming that there has been a systematic fractional shift Δ of the entire profile; i.e., at each atmospheric pressure level p, the water content has changed by the same relative amount Δ:

$$H_2O'(p) = (1+\Delta)H_2O(p) \qquad (7)$$

To illustrate, examine Figures 1 and 2. Figure 1 shows three water vapor profiles obtained on different days from Hobart radiosonde measurements giving water concentration as a function of height. In Figure 2 we replot the "midrange" curve from Figure 1 together with its family of adjusted profiles generated by multiplying the water concentration at each height by a scale factor $k = 1 + \Delta$. Setting $k = 1$ (i.e., $\Delta = 0$) corresponds to no change; for $0 \le k < 1$, the water concentration has been reduced, and for $k > 1$, it has been increased. Setting $k = 2$, for example, doubles the concentration at each radiosonde sample height; setting $k = 0.8$ reduces water content to 80% of the original.

3. Use LOWTRAN 7 to calculate the revised transmissivity $\tau_{v,\infty}'$ and atmospheric radiance $B_v'(\overline{T}_a)$ for the new water profile. Substitute these in (1) to produce the radiance pair (I_4', I_5'); this is the predicted satellite observation when the water vapor profile has been changed by Δ.

4. Substitute the satellite radiance pair (I_4', I_5') and the original prescribed coefficients of step 1 into (1), solve for the pair of surface radiances ($B_4(T_s)$, $B_5(T_s)$), and then invert the blackbody function using the channel 4 and 5 central wavenumbers to map to the corresponding pair of surface temperature estimates ($T_{s,4}$, $T_{s,5}$). Obviously, these two temperature estimates will not be equal, since this step simulates the (usual) situation of having a fixed algorithm whose assumed atmospheric profile does not match the ac-
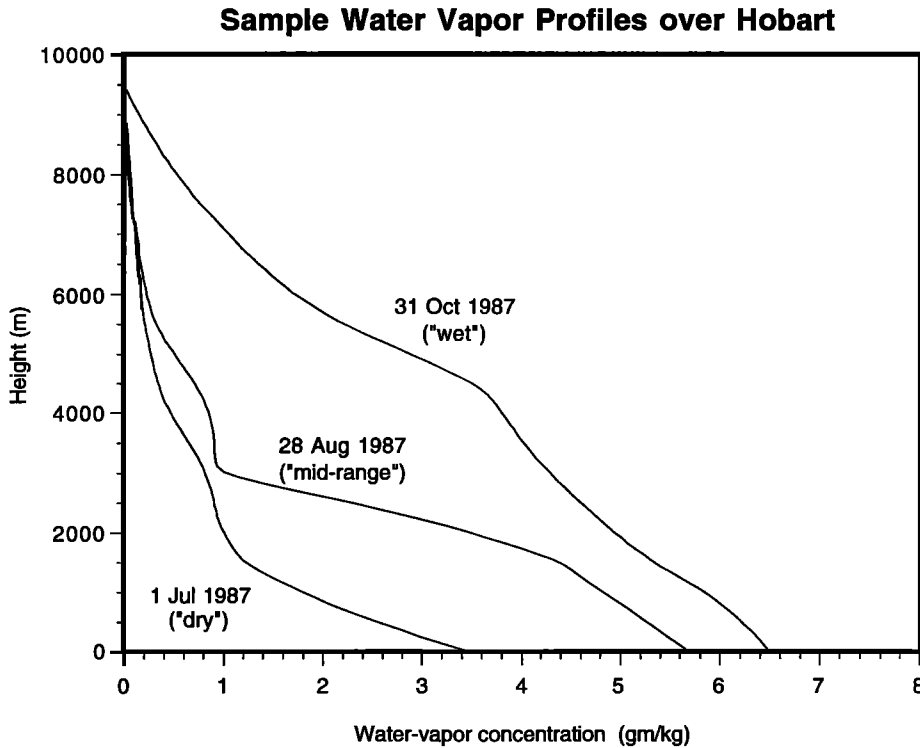

Fig. 1. Sample water vapor profiles from radiosondes released from Hobart, showing the large variation in both the profile shape and total water content over a 4-month interval. Water content (mixing ratio) is recorded as grams of water vapor per kilogram of air.
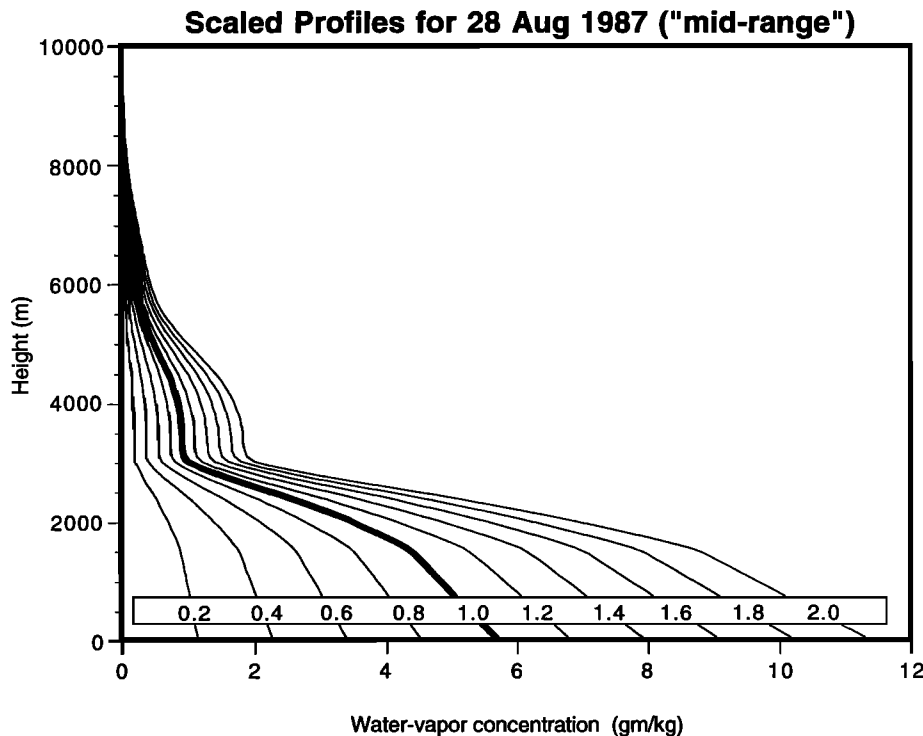
Fig. 2. Family of adjusted water vapor profiles for the middle curve of Figure 1. The numeric value attached to each profile gives the concentration multiplier $k = 1 + \Delta$. The heavy curve ($k = 1.0$) is the original unadjusted profile from Figure 1.

tual profile. This nonzero difference $\Delta\text{SST} = (T_{s,4} - T_{s,5})$ establishes the correspondence between ΔSST and ΔH_2O.

Repeat steps 2 to 4 for a range of water profile shifts (typically, $0 < k < 2.5$), and compile a six-column table with column headings ΔH_2O, ΔSST, $B_4'(\overline{T}_a)$, $B_5'(\overline{T}_a)$, $\tau_{4,\infty}'$, and $\tau_{5,\infty}'$.

A sample DWV correction table for August 28, 1987, is shown in Table 1. In Figure 3 we plot the first two columns of three such DWV tables for the representative profiles illustrated in Figure 1. We see that within LOWTRAN 7 modeling errors, all three correction curves pass through the point $(k, \Delta\text{SST}) = (1.0, 0.0)$, corresponding to the original unmodified water profiles. As k increases, ΔSST increases monotonically, supporting our fundamental conjecture that ΔSST is a reliable measure of how far the actual water vapor profile deviates from the assumed profile. For the limited range of k values likely to be encountered over a typical AVHRR image, the curvatures evident in the trend lines would probably be adequately modeled as linear.

Applying the DWV Method to Retrieve SST

Having generated the water vapor correction table using steps 1 to 4, our retrieval algorithm proceeds as follows.

5. Ensure that the pixel in question is cloud-free. Convert the raw AVHRR count to satellite radiance for channels 4 and 5 (calibration procedures are outlined in the next section).

6. Use satellite radiances and (1) with the prescribed coefficients $\tau_{v,\infty}^0$ and $B_v^0(\overline{T}_a)$ to obtain $(T_{s,4}, T_{s,5})$ and thus ΔSST (per step 4 above).

7. Use ΔSST as an index to the water vapor correction table to infer first-guess values for ΔH_2O, corrected atmospheric radiances $B_v'(\overline{T}_a)$, and corrected transmissivities

$\tau_{v,\infty}'$. Substitute these along with satellite radiances I_v into (1), solve for sea surface radiances $B_v(T_s)$, and hence deduce the improved ΔSST error estimate.

8. Select several table entries on either side of the initial ΔH_2O guess, and repeat step 7. The iteration which minimizes $|T_{s,4} - T_{s,5}|$ is taken as providing the best SST estimate. Typically, we find that the resulting surface temperature estimates $T_{s,4}$ and $T_{s,5}$ agree to within ±0.05 K, so split the difference for a final SST of $(T_{s,4} + T_{s,5})/2$.

Shown circled in Figure 3 are the optimal k adjustments required to null the ΔSST retrieval in the buoy pixel for each of the 3 days. (In Section 4 we evaluate the quality of 33 DWV-compensated SST retrievals by comparing them with actual buoy measurements.) The circled datum defines a local "operating point" on the ΔSST versus ΔH_2O curve for a given day. Following steps 5 through 8 to apply the DWV technique to a full AVHRR image would see the operating point gradually move up or down the curve as the algorithm attempts to compensate for variations in ΔSST by fine-tuning the atmospheric water content.

Having obtained the optimal ΔH_2O adjustment, it is a straightforward matter to compute the total water content between satellite and ocean surface for a given pixel by integrating the modified water profile as a function of height. In addition, we can deduce the average atmospheric temperature by inverting the selected atmospheric radiance entry in the DWV table. For example, in Table 1 the second row marked with asterisks ($k = 1.28$) shows atmospheric radiances for channels 4 and 5 of 6.3×10^{-4} and 6.23×10^{-4} W/(cm² sr μm) respectively. Inverting the blackbody function using the central wavelength produces an average atmospheric temperature estimate across the two channels of $1.4° \pm 0.3°\text{C}$, which is more than 10°C lower than either the DWV-compensated SST (12.03°C) or the actual buoy temperature

TABLE 1. Sample DWV Table for August 28, 1987 (Midrange Water Profile)

$(1+\Delta)H_2O$	ΔSST	$B_4(\overline{T}_a)/10^{-4}$	$B_5(\overline{T}_a)/10^{-4}$	τ_4	τ_5
0.90	-0.121	6.200	6.148	0.8259	0.7635
0.92	-0.097	6.214	6.154	0.8215	0.7572
0.94	-0.061	6.224	6.160	0.8170	0.7508
0.96	-0.030	6.234	6.166	0.8124	0.7444
0.98	-0.009	6.244	6.171	0.8078	0.7380
1.00*	0.031*	6.253*	6.176*	0.8032*	0.7314*
1.02	0.052	6.262	6.181	0.7985	0.7249
1.04	0.081	6.270	6.186	0.7938	0.7183
1.06	0.118	6.279	6.191	0.7890	0.7116
1.08	0.161	6.287	6.195	0.7841	0.7049
1.10	0.165	6.295	6.199	0.7793	0.6982
1.12	0.210	6.302	6.203	0.7744	0.6914
1.14	0.229	6.309	6.207	0.7694	0.6846
1.16	0.262	6.316	6.211	0.7643	0.6777
1.18	0.299	6.323	6.214	0.7593	0.6709
1.20	0.342	6.329	6.217	0.7542	0.6640
1.22	0.352	6.336	6.220	0.7491	0.6571
1.24	0.399	6.342	6.223	0.7440	0.6501
1.26	0.428	6.347	6.226	0.7388	0.6432
1.28*	0.448*	6.353*	6.229*	0.7335*	0.6362*
1.30	0.467	6.358	6.231	0.7283	0.6292
1.32	0.522	6.363	6.233	0.7230	0.6222
1.34	0.523	6.368	6.236	0.7177	0.6152
1.36	0.588	6.373	6.238	0.7123	0.6081
1.38	0.604	6.378	6.240	0.7069	0.6011

This coarsely sampled subset of the ΔSST versus $(1+\Delta)H_2O$ look-up table was created using the DWV algorithm, steps 1 through 4. The $B_v(\overline{T}_a)$ atmospheric radiance columns have units of $W/(cm^2 \, sr \, \mu m)$.

* These are the initial prescribed coefficients (for $k = 1.00$) and the final iteratively-optimized coefficients (for $k = 1.28$) for the buoy pixel on this day. The fact that the initial ΔSST of 0.031 is not precisely zero indicates to us that the LOWTRAN 7 transmission model is slightly imperfect.
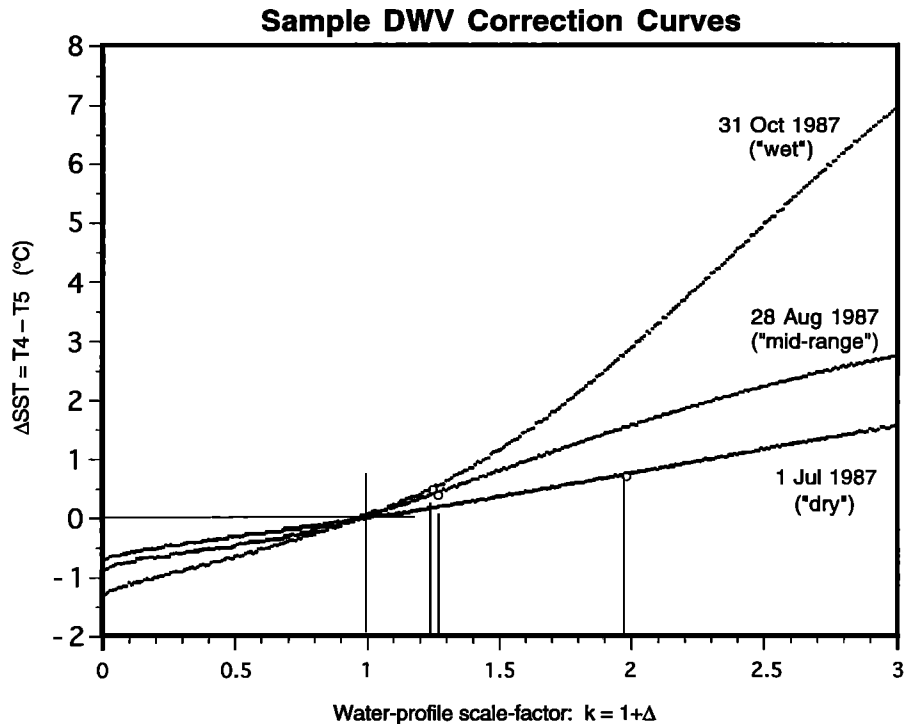

Fig. 3. Predicted sea surface temperature (SST) mismatch as a function of water content adjustment for the three profiles of Figure 1. The circled points show the optimal k adjustment required to null the ΔSST in the AVHRR retrieval for the buoy pixel on the given day.

(11.5°C). We find that for our coastal test site the average atmospheric temperature is consistently colder than the sea temperature (compare the buoy and T_a columns of Table 2).

3. THE TEST DATA SET

The region of interest was defined by the position of a WaveRider buoy moored off the west coast of Tasmania at location 145°9.4'E, 42°8.7'S, as shown in Figure 4, for the period April 27 to December 21, 1987. The buoy measured the sea temperature every 12 min on an ongoing basis to an absolute accuracy of ±0.1°C or better. The effective depth of the temperature-sensing element was approximately 32 cm below the surface. The range of temperatures recorded by the buoy over this time was 10°–15°C.

The full suite of NOAA 9 AVHRR "quick-look" images received by the Commonwealth Scientific and Industrial Research Organisation (CSIRO) Marine Laboratories in Hobart for this time period were inspected, and 41 passes

which appeared to be cloud-free over the buoy region were selected for further examination. To accurately locate the buoy pixel for each of these 41 raw-space (i.e., satellite line versus pixel) images, a coastline of Tasmania was mapped from latitude/longitude to raw-image coordinates, and the spacecraft attitude parameters (roll, pitch, yaw) were fine-tuned to maximize the correlation between coastline and the image. This optimized latitude/longitude to raw-space transformation was then applied to the known buoy latitude/longitude position to yield its raw line/pixel location. A multichannel sub image of 400 by 400 pixels centered on this buoy position was then extracted.

Atmospheric profiles (pressure, temperature, water content) for the region were extracted from an archive of twice-daily radiosonde balloon flights which were released from Hobart, 200 km southeast of the buoy position. The archive was acquired from the Melbourne Bureau of Meteorology. Unfortunately, temporally coincident sonde data are available for only the first 35 of our selected 41 passes, so we

TABLE 2. Comparison of DWV Performance with M4 and CPSST

	IFUT	Date in 1987	Buoy °C	(Buoy − SST$_{pred}$) DWV	(Buoy − SST$_{pred}$) M4	(Buoy − SST$_{pred}$) CPSST	U, g/cm^2	T_a, °C
1	m9jr	May 9	13.83	−0.57	0.44	0.49	1.71	3.48
2	m9k5	May 10	13.89	−0.86	0.34	0.35	2.05	6.62
3	m9kc	May 10	14.11	−0.15	0.99	0.42	1.54	5.89
4	m9n9	May 18	13.76	0.36	1.90	1.52	2.04	1.81
5	m9na	May 18	13.74	−0.40	0.66	0.82	1.66	1.71
6	m9vi	Jun. 8	12.73	−0.05	1.03	0.91	1.14	−0.20
7	ma4c	Jun. 30	12.08	1.00	2.06	1.59	0.84	−5.19
8	ma4i	Jul. 1	11.45	0.07	0.99	1.25	1.24	−4.18
9	mabk	Jul. 19	10.77	−0.36	0.56	0.80	1.08	−4.63
10	mabz	Jul. 20	11.21	0.42	1.53	1.61	1.57	−3.58
11	mac6	Jul. 20	12.40	0.22	1.29	0.77	0.84	−5.11
12	macc	Jul. 21	11.12	−0.55	0.56	0.73	1.66	−1.59
13	macd	Jul. 21	11.35	0.73	1.51	2.04	1.48	−1.73
14	macq	Jul. 22	11.91	1.16	2.27	2.45	1.87	−1.09
15	macr	Jul. 22	11.64	−0.18	0.87	1.02	1.14	−1.95
16	mad5	Jul. 23	11.32	0.20	1.18	1.24	0.83	−4.93
17	maeb	Jul. 26	13.08	0.66	1.37	1.78	1.30	−3.30
18	maep	Jul. 27	12.88	0.97	1.61	2.47	1.92	−2.10
19	maf3	Jul. 28	13.08	0.60	1.48	1.87	1.33	−0.71
20	mafh	Jul. 29	12.46	0.47	1.32	1.54	1.30	−3.43
21	mafw	Jul. 30	11.84	−0.03	0.98	1.11	2.03	2.13
22	mald	Aug. 13	11.19	−0.12	0.78	0.77	1.01	−0.23
23	malk	Aug. 13	11.74	−0.11	0.90	0.51	1.94	1.43
24	mar9	Aug. 28	11.50	−0.54	0.46	0.64	1.71	1.41
25	mazo	Sep. 18	12.19	−0.19	0.76	0.40	1.98	5.59
26	mb11	Sep. 22	12.08	0.01	0.67	0.87	2.70	6.12
27	mb1f	Sep. 23	12.33	0.13	0.68	0.67	1.67	0.83
28	mb1n	Sep. 23	12.50	0.11	0.69	0.30	1.18	0.55
29*	mb21	Sep. 24	12.65	9.40*	2.56	2.39	5.47*	9.65*
30	mb2m	Sep. 26	12.39	0.28	0.54	0.63	2.65	7.94
31	mb9o	Oct. 14	10.01	0.43	1.23	1.52	2.06	4.87
32	mbdz	Oct. 25	12.42	1.99	2.62	3.03	1.99	3.63
33	mbg5	Oct. 30	15.11	0.86	1.40	1.19	1.62	8.18
34	mbgc	Oct. 31	14.59	0.76	0.48	0.59	2.80	8.85
Bias				0.22	1.10	1.15		
rms				0.59	0.56	0.68		
N				33	33	33		

The IFUT (image file utility number) is a unique four-character satellite pass identifier used by the Hobart ground station. The columns headed U and T_a are the DWV estimates for vertical water column (g/cm^2) and slant path average atmospheric temperature, respectively. N is number of samples.

* For mb21 (pass 29), DWV failed dramatically, producing the unphysical result $T_a > $ SST (see text and Table 4). This pass was excluded from the bias and rms statistics.
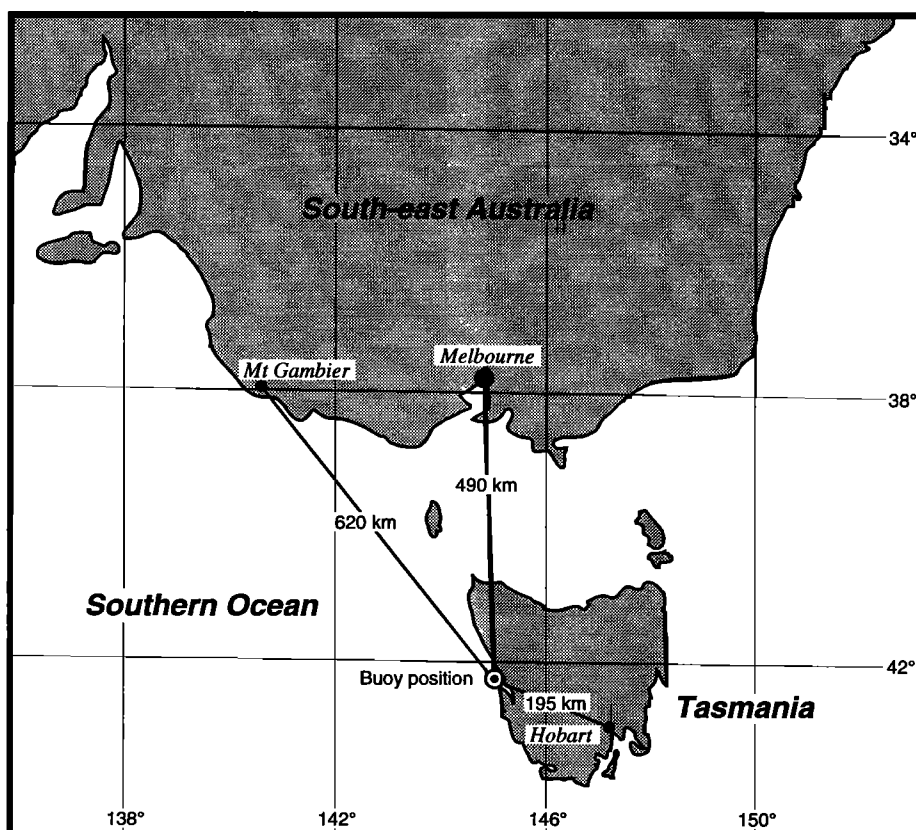
Fig. 4. Locations of the buoy and the three radiosonde sites: Hobart, Mount Gambier, and Melbourne.

had to drop the remaining six AVHRR images from our "full physics" analysis. One further image was omitted when we discovered that the satellite overpass occurred in the middle of a 3-hour break in the buoy temperature record.

4. ANALYSIS AND RESULTS

For each of the surviving 34 subimages, we extracted the raw channel 4 and channel 5 counts (averaged over a 3-pixel by 3-pixel box to reduce digitization effects) for the buoy pixel, converted counts to radiance using the in-flight calibrations to provide a linearized first estimate, and then applied the nonlinearity correction directly in radiance space using the "a method" described by Steyn-Ross et al. [1992a,b].

To implement our DWV method, we customized the LOWTRAN 7 "midlatitude winter" standard atmosphere by ingesting the Hobart radiosonde (temperature, pressure, water vapor) and specified the satellite scan angle (computed from the pixel number) so that LOWTRAN 7 would compute the transmissivities for the slant path. We then followed steps 1 to 4 described above to generate a finely stepped ΔSST-versus-ΔH_2O correction look-up table, thus simulating the effect of a buoy atmosphere which was wetter (or drier) than the Hobart sounding. Once the table was complete, the calibrated pair of satellite radiances were substituted into (1) to obtain ΔSST = $(T_{s,4} - T_{s,5})$, giving the initial entry point into the table. The table was then scanned in the vicinity of the entry point to find the water vapor adjustment which minimized the $T_{s,4} - T_{s,5}$ difference, thus producing a final SST estimate.

This table-generating/table-scanning procedure was repeated for each of the 34 subimages. The resulting scatterplot of DWV-compensated SST estimate versus buoy temperature is shown in Figure 5a. By way of comparison, the standard McMillin and Crosby [1984] M4 MCSST model (as implemented by the CSIRO-Hobart Remote Sensing group) predictions are shown in Figure 5b, and the NESDIS CPSST [Walton et al., 1990] predictions appear in Figure 5c. (The M4 and CPSST equations are listed in the appendix.)

To quantify algorithm performance, we define error as buoy temperature minus SST estimate, and compute the mean error (i.e., the bias) and the standard deviation of the errors (the rms error). We see from Table 2 and Figures 5a, 5b, and 5c that on average, the DWV method underestimates the buoy temperature by 0.22 K, whereas for the M4 and CPSST models, the biases are 1.10 and 1.15 K, respectively. The DWV result is most encouraging, since the 0.22 K differential is of the correct sign and magnitude if we assume that the skin effect produces a temperature lowering in the accepted range of 0.2 to 0.5 K [Robinson et al., 1984]; i.e., the skin temperature (sensed by the radiometer) is expected to underestimate the bulk temperature (sensed by the buoy) by 0.2–0.5 K.

All three models display a similar amount of scatter as measured by rms error (0.59, 0.56, and 0.68 K for DWV, M4, and CPSST respectively). We consider that this is probably an indication of the inherent noise in the preflight and in-flight calibrations of the radiometer.

For 33 of the 34 satellite passes, the DWV method, using the Hobart radiosondes, produced SST estimates which were consistently close to the buoy temperature. One pass (mb21;
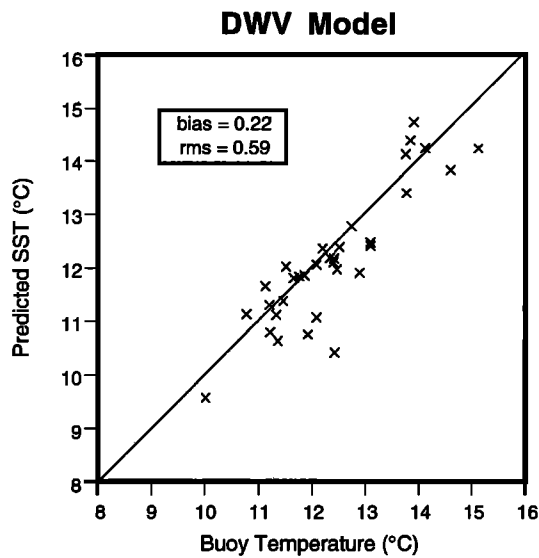
DWV Model

Fig. 5a. Scatterplot of dynamic water vapor-compensated SST versus ocean buoy temperature for 33 samples gathered over a 6-month period in 1987 (see Table 2).

see Tables 2 and 4), however, predicted an SST of 3.25°C, which is 9 K lower than ground truth. This clearly spurious result arises, we believe, from markedly different atmospheric conditions between the buoy site and the Hobart radiosonde station. (Inspection of the satellite image for this pass shows heavy cumulus cloud above Hobart but clear skies above the buoy pixel.) This failing pass was excluded from the summary statistics.

Also shown in Table 2 are the DWV-compensated estimates for U, the total vertical water vapor column, and $\overline{T_a}$, the average atmospheric temperature along the pixel-to-satellite slant path (obtained by inverting the LOWTRAN 7 returned atmospheric radiance). The LOWTRAN 7 estimate for the iterated water vapor column is also for the slant path; we converted this to a vertical amount by using the approximate relationship $U = U_{\text{slant}} \cos\phi$, where ϕ is the satellite scan angle (this formula neglects Earth curvature and optical refraction effects).
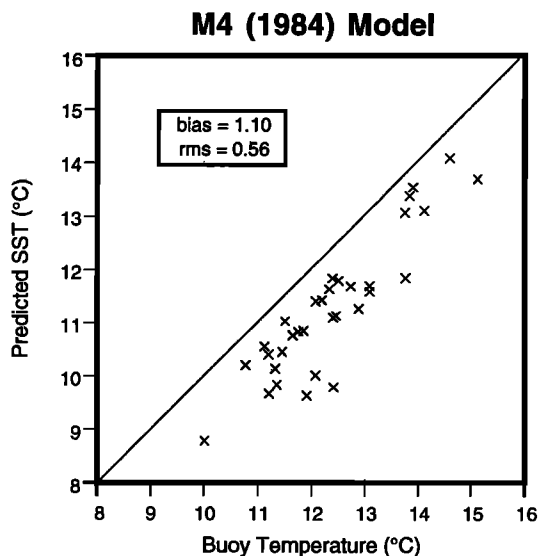
M4 (1984) Model

Fig. 5b. Scatterplot of M4 MCSST predictions [McMillin and Crosby, 1984] for the same 33 samples listed in Table 2.
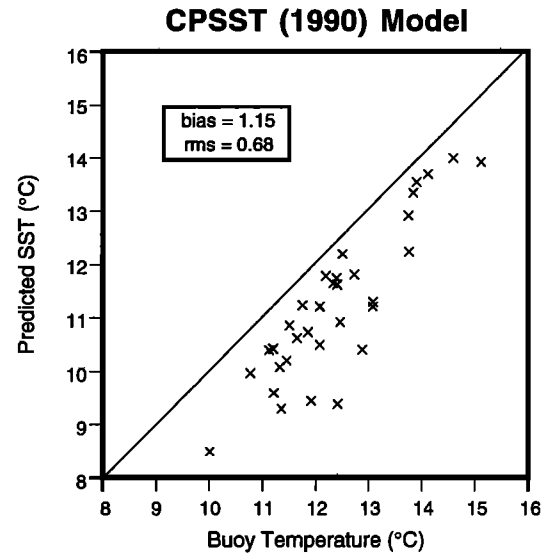
CPSST (1990) Model

Fig. 5c. Scatterplot of 33 CPSST predictions [Walton et al., 1990].

To check the sensitivity of the DWV method to the choice of assumed temperature profile, we repeated our SST retrieval analysis using radiosondes from two sites on the Australian mainland, namely, Mount Gambier (620 km northwest of the buoy) and Melbourne (490 km north) (see Figure 4). These stations have ground temperatures which, when averaged over the period of interest, are 1 and 2.5 K warmer, respectively, than those at Hobart. Despite this temperature difference, the first three columns of Table 3 show that the quality of the DWV SST predictions from the two warmer, more distant sites is very similar to that from the Hobart site. Table 3 also shows intercomparisons between the three sonde sites for DWV-predicted vertical water vapor amount and slant path atmospheric temperature. In the absence of buoy pixel truth for water vapor and atmospheric temperature, these intercomparisons suggest that the DWV returns for the buoy pixel water column are reasonably consistent, while the DWV-adjusted $\overline{T_a}$ estimates seem to be more a reflection of the temperature profile at the sounding site than an extrapolation to the buoy site.

Table 3 contains the statistics for only the first 26 of the 34 passes; the last eight passes were excluded because for the Melbourne site, soundings were unavailable for the final four and the DWV failed on the preceding four passes. Table 4 shows that the group of four Melbourne failures brackets the already identified Hobart mb21 failure and matches up with a cluster of Mount Gambier failures, suggestive of a strong weather system moving from west to east over the sonde sites which left the buoy site with clear skies (all 34 images were cloud-free over the buoy pixel). This severe weather hypothesis is presently being investigated. Interestingly, all eight pathological cases (one for Hobart, three for Mount Gambier, and four for Melbourne) predicted an SST which was lower than the DWV-adjusted atmospheric temperature, the reverse of what we would normally expect. This inversion may provide a convenient automatic flag that the method has failed.

5. DISCUSSION

Although the preliminary results for the DWV method are very promising, there is considerable scope for improve-

TABLE 3. Comparison of 26 DWV Predictions from Three Radiosonde Sites

	SST Error, °C			Water Vapor Difference ΔU g/cm^2			Atmospheric Temperature Difference, ΔT_a °C		
	Buoy – 74	Buoy – 21	Buoy – 86	21 – 74	86 – 74	21 – 86	21 – 74	86 – 74	21 – 86
Bias	0.11	0.15	0.12	0.25	0.25	0.00	1.35	1.82	-0.46
rms	0.53	0.52	0.61	0.34	0.25	0.18	1.75	2.23	1.95

The radiosonde site identifiers are 74 for Hobart, 21 for Mount Gambier, and 86 for Melbourne (see Figure 4). The last eight of the 34 passes listed in Table 2 have been excluded from the analysis (see text). For the first 26 passes, DWV was able to use soundings from each of the three sites to predict the buoy pixel SST equally well. The DWV-adjusted total water vapor estimates are consistent for the west/east pairing of Mount Gambier/Melbourne, but less so for the north/south station pairings. The DWV-adjusted atmospheric temperature returns are more variable.

ment, particularly in the way in which the water profiles are adjusted. Our rather crude approach of using a simple multiplicative factor to scale up the water content ignores the fact that at high humidity levels such a simple-minded scaling can easily produce relative humidity levels in excess of 100%, corresponding to the rather unphysical situation of supersaturated air. Such unphysical transgressions are duly flagged by LOWTRAN 7; fortunately, the program is able to proceed with the transmissivity calculations. A better approach might be to tune the water profile by adding fractional amounts of an average reference water vapor profile and to incorporate feasibility checks to ensure that humidity levels do not exceed 100%.

The fact that the DWV technique converged to a reasonable value for the SST in 33 of 34 cases (using Hobart soundings), despite our simple-minded water adjustment method, suggests that ΔSST mismatch is not particularly sensitive to the precise shape of the water profile but instead depends strongly on the total water vapor content.

For the 33 passes, the median water vapor adjustment factor $k = 1 + \Delta$ was 1.3, indicating that on average the Hobart water profile had to be scaled up by about 30% to minimize the $T_{s,4} - T_{s,4}$ difference over the buoy pixel. Only two passes required a reduction in water concentration (by -1% and -6%). Two passes required no adjustment at all, and three passes needed an approximate doubling of water content ($k = 1.99$, 2.03, 2.29). The median adjustment is consistent with the intuitive notion that the profile over coastal Hobart is likely to be drier than the profile over the ocean buoy, particularly at low altitudes.

When comparing the relative performance of DWV with published MCSST and CPSST models, we have deliberately not made any attempt to regression-tune the M4 and CPSST

coefficients, as this would predictably produce SST estimates with a zero bias for this region only. Rather, our method is regression-free and thus could be applied to any geographical location for which a nearby radiosonde is available. Regression-based methods can be expected to perform well only in the region for which they have been customized.

SUMMARY

This paper has presented a new SST retrieval technique which dynamically tunes the algorithm coefficients to compensate for temporal amospheric water vapor fluctuations. The basis of our method is the notion that any single-channel, fixed-coefficient method can yield identical SST estimates from two distinct AVHRR channels (4 and 5) only if the atmospheric profile used to obtain the algorithm coefficients is the same as the actual amosphere sensed by the satellite. Conversely, if the pair of channel 4 and 5 SST predictions are not identical, then the temperature mismatch ΔSST $= T_{s,4} - T_{s,4}$ provides a measure of how much the assumed and actual atmospheres differ. Since water vapor variations constitute the most rapidly varying atmospheric component, we assert that this ΔSST mismatch primarily arises from water vapor variations, which we denote by ΔH_2O.

Our assertion is supported by simulating the water vapor variations in actual atmospheres. These simulations reveal a monotonic, almost linear relationship between ΔSST and ΔH_2O (Figure 3). Using this relationship, we have established a procedure which would adjust the assumed water vapor profile for each pixel in the AVHRR scene. When compared with buoy ground truth, we find that such profile tuning results in SST estimates which are more accurate than those typically obtained from fixed-coefficient algorithms.

TABLE 4. Time Series of DWV Failures

	IFUT	Date in 1987	Sonde 74: Hobart			Sonde 21: Mt.Gambier			Sonde 86: Melbourne		
			SST, °C	T_a, °C	U, g/cm^2	SST, °C	T_a, °C	U, g/cm^2	SST, °C	T_a, °C	U, g/cm^2
25	mazo	Sep. 18	12.4	5.6	2.0	12.1	8.3	3.1	11.6	8.4	3.0
26	mb11	Sep. 22	12.1	6.1	2.7	12.1	8.1	4.0	13.1	7.4	3.4
27	mb1f	Sep. 23	12.2	0.8	1.7	-8.3*	9.5*	6.7*	-45.8*	9.4*	7.8*
28	mb1n	Sep. 23	12.4	0.6	1.2	8.6*	10.9*	5.5*	7.8*	10.8*	6.2*
29	mb21	Sep. 24	3.3*	9.7*	5.5*	-9.9*	9.5*	7.1*	-273.2*	9.5*	11.1*
30	mb2m	Sep. 26	12.1	7.9	2.7	12.1	6.3	2.2	8.5*	10.9*	4.8*
31	mb9o	Oct. 14	9.6	4.9	2.1	9.6	4.3	2.0	–	–	–

*The DWV method occasionally failed producing a dramatically lowered SST and a vastly exaggerated water column estimate for the buoy pixel. The more distant radiosonde sites are more prone to DWV collapse. These failures are temporally and geographically correlated, suggesting unusually large atmospheric temperature gradients between sonde station and buoy site, possibly due to severe weather patterns. (There were no Melbourne sonde data available for the mb90 or later passes.) The IFUT is the pass identifier defined in Table 2.

DWV is a physics-based method which does not rely on any form of AVHRR versus ground truth regression, so in principle it could be applied to any coastal or ocean region. Fixed-coefficient algorithms typically do not perform well over coastal areas [McMillin and Crosby, 1984] because of the high variability of atmospheric conditions near land masses. To the extent that water vapor changes are the dominant fluctuating component, a DWV approach will better accommodate these local variabilities.

Enhanced SST accuracies are of particular interest to climate modelers. For example, the international Tropical Ocean Global Atmosphere program has set SST accuracy requirements at 0.3 K. At best, typical SST algorithms can provide an accuracy of 0.7 K at midlatitudes [Barton, 1985]. The dynamic water vapor correction method has the potential to trim this figure by a substantial margin and, by implementing the improvements discussed earlier, should be able to achieve the stringent accuracy levels required by climate modelers. We also note that DWV yields an estimate for total water vapor content, another significant quantity for global climate change with applications to surface flux calculations. These water vapor estimates are at AVHRR pixel resolution rather than the coarser resolutions available from microwave radiometers (e.g., Special Sensor Microwave Imager (SSMI)).

We expect to be able to refine the DWV method by using a more precise transmission model, by incorporating a more physically realistic description of the vertical variation of water vapor in the atmosphere, and by making use of coincident profiles over sea rather than nonlocal radiosondes from a nearby coast.

If the water vapor model is to be made operational, one would need to update the ΔH_2O versus ΔSST look-up tables on, say, a daily or weekly basis. The reward for the computational effort implicit in our method would be that one could retrieve estimates for water vapor content of the atmosphere and SSTs which have been corrected for water vapor. This represents rather more information than is available from standard SST methods, so this new approach may be of interest to the climate-modeling community.

APPENDIX

The coefficients for the M4 MCSST algorithm were derived by McMillin and Crosby [1984]. Given the channel 4 and 5 brightness temperatures (in Kelvin), (A1) returns the SST estimate (in Kelvin). Note that there is no slant path correction.

$$SST = T_4 + 2.702(T_4 - T_5) - 0.582 \qquad (A1)$$

The CPSST split-window algorithm [Walton et al., 1990] provides separate equations for day and night passes. The returned SST estimate is in degrees Celsius:

$$SST_{day} = \frac{0.19069T_5 - 49.16}{0.20524T_5 - 0.17334T_4 - 6.78}(T_4 - T_5 + 0.789)$$
$$+ 0.92912T_5 + 0.81(T_4 - T_5)(\sec\theta - 1) - 254.18$$

$$\qquad (A2)$$

$$SST_{night} = \frac{0.19596T_5 - 48.61}{0.20524T_5 - 0.17334T_4 - 6.11}(T_4 - T_5 + 1.46)$$
$$+ 0.95476T_5 + 0.98(T_4 - T_5)(\sec\theta - 1) - 263.84$$

$$\qquad (A3)$$

where θ is the local zenith angle.

REFERENCES

Barton, I. J., Transmission model and ground-truth investigation of satellite-derived sea surface temperatures, *J. Clim. Appl. Meteorol.*, 24, 508–516, 1985.
Barton, I. J., A. M. Zavody, D. M. O'Brien, D. R. Cutten, R. W. Saunders, and D. T. Llewellyn-Jones, Theoretical algorithms for satellite-derived sea surface temperatures, *J. Geophys. Res.*, 94, 3365–3375, 1989.
Kneizys, F. X., E. P. Shettle, L. W. Abreu, J. H. Chetwynd, G. P. Anderson, W. O. Gallery, J. E. A. Selby, and S. A. Clough, Users guide to LOWTRAN 7, *Rep. AFGL-TR-88-0177*, 137 pp., Air Force Geophys. Lab., Hanscom Air Force Base, Mass., 1988.
McClain, E. P., W. G. Pichel, and C. C. Walton, Comparative performance of AVHRR-based multichannel sea surface temperatures, *J. Geophys. Res.*, 90, 11,587–11,601, 1985.
McMillin, L. M., and D. S. Crosby, Theory and validation of the multiple window sea surface temperature technique, *J. Geophys. Res.*, 89, 3655–3661, 1984.
Robinson, I. S., N. C. Wells, and H. Charnock, The sea surface boundary layer and its relevance to the measurement of sea surface temperature by airborne and spaceborne radiometers, *Int. J. Remote Sens.*, 5(1), 19–45, 1984.
Steyn-Ross, D. A., M. L. Steyn-Ross, and S. Clift, Radiance calibrations for advanced very high resolution radiometer infrared channels, *J. Geophys. Res.*, 97, 5551–5568, 1992a.
Steyn-Ross, D. A., M. L. Steyn-Ross, S. Clift, and J. Shepherd, Radiance calibrations for NOAA-9 AVHRR infrared channels, *Proc. Sixth Australas. Remote Sens. Conf.*, 3, 222–230, 1992b.
Walton, C. C., Nonlinear multichannel algorithms for estimating sea surface temperature with AVHRR data, *J. Appl. Meteorol.*, 27(2), 115–124, 1988.
Walton, C. C., E. P. McClain, and J. F. Sapper, Recent changes in satellite based multichannel sea surface temperature algorithms, Marine Technology Society, preprint MTS 90, Washington D.C., 1990.

J. Reid and P. Tildesley, CSIRO Division of Oceanography, GPO Box 1538, Hobart, Tasmania 7001, Australia.
J. D. Shepherd, P. J. Smith, D. A. Steyn-Ross, and M. L. Steyn-Ross, Physics Department, University of Waikato, Private Bag 3105, Hamilton, New Zealand.